Single photon emission from deep-level defects in monolayer WSe_2

Yanxia Ye, Xiuming Dou,* Kun Ding, Yu Chen, Desheng Jiang, Fuhua Yang, and Baoquan Sun†

State Key Laboratory of Superlattices and Microstructures, Institute of Semiconductors, Chinese Academy of Sciences, Beijing 100083, China

(Received 15 November 2016; revised manuscript received 18 April 2017; published 26 June 2017)

We report an efficient method to observe single photon emissions in monolayer WSe_2 by applying hydrostatic pressure. The photoluminescence peaks of typical two-dimensional excitons show a nearly identical pressure-induced blueshift, whereas the energy of pressure-induced discrete emission lines (quantum emitters) demonstrates a pressure insensitive behavior. The decay time of these discrete line emissions is approximately 10 ns, which is at least one order longer than the lifetime of the broad localized (L) excitons. These characteristics lead to a conclusion that the excitons bound to deep-level defects can be responsible for the observed single photon emissions.

DOI: 10.1103/PhysRevB.95.245313

Unlike luminescence centers in traditional three-dimensional semiconductors which are located away from the surface, quantum emitters in atomic thin transition-metal dichalcogenide semiconductors such as WSe_2 and hexagonal boron nitride have been observed at the edges or vacancies of the flakes [1–9]. Local strain gradients which occur at the edges are considered to modulate the electronic states of the localized excitons [2,9–11], resulting in spatially and spectrally isolated single photon emission. This means that strain engineering is an effective approach to obtain spatially and spectrally isolated quantum emitters in two-dimensional (2D) semiconductors. However, the uncontrollability of strains as reported requires one to better understand and explore the electronic and optical properties of discrete emitters. Therefore, *in situ* strain tuning becomes essential for understanding the optical properties of discrete emitters.

Here, we present an effective method to give rise to single photon emission lines in monolayer WSe_2 and provide experimental evidence to show that the deep-level defects should be responsible for the single photon emissions. The results are based on the application of hydrostatic pressure technique in the low-temperature photoluminescence (PL) measurement of monolayer WSe_2. The 2D excitons and discrete emission lines which arise during pressure application are studied in detail by the pressure-dependent PL and time-resolved PL (TR-PL). The pressure is introduced by the piezoelectric (PZT) actuator-driven diamond-anvil cell (DAC) device for *in situ* pressure tuning. In addition to the pressure coefficients (PCs) of the 2D excitons, the abnormal pressure responses of the discrete lines are observed. The characteristics of the discrete emission lines have been carefully checked by measurements before and after the pressure engineering cycles.

In our experiments, monolayer WSe_2 flakes were prepared by micromechanical exfoliation from a bulk WSe_2 (*2D semiconductors* supplied) on a thinned SiO_2/Si substrate. Monolayer samples are identified by microscopic image contrast and room temperature PL spectra, as shown in Fig. 1, together with the PL spectra of bilayer and trilayer. They show typical thickness-dependent PL line shapes and peak energies. In this paper, we only focused on the pressure-induced single photon emissions of monolayer WSe_2. A high pressure can be applied to the measured samples by using a DAC device driven by a PZT actuator [12]. Condensed argon was used as the pressure-transmitting medium, and the ruby R_1 fluorescence line shift was used to determine pressure. The calibrated temperature of the cryogenic DAC sample chamber is 20 K. The PL was collected by a 20× objective (NA: 0.35) and spectrally analyzed using a 0.5 monochromator equipped with a silicon charge-coupled device at an excitation of tens of microwatts by a continuous wave (cw) or pulse adjustable 640 nm semiconductor laser. Silicon single photon counting modules with a time resolution of 380 ps were used for time-resolved PL and the second-order correlation function $g^{(2)}(\tau)$ measurements.

When the laser excitation spot is focused on the central region of the monolayer WSe_2 flakes, typical PL peaks of the 2D neutral exciton (2D-X^0), 2D charge exciton (2D-X^-), and defect-related L exciton band at 20 K are observed at zero pressure [13–15], as shown in Figs. 2(a) (sample 1) and 2(b) (sample 2). Figure 2(a) shows the PL spectral curves measured at the pressures of 0.83, 1.51, 1.98, 2.32, and 4.4 GPa, respectively, showing that 2D exciton emission peaks disappear and discrete lines emerge under high pressure. Here, PL spectra were measured at low temperature, while the pressure-increasing process should be achieved at room temperature. Therefore, we cannot confirm that the laser excitation spot regions are exactly the same under the different pressures. This maybe results in the arbitrary distributions of discrete lines observed. However, it is found that, even though the laser excitation spot focuses on the exact same position of the sample during the applied pressure process by *in situ* changing pressure at low temperature, the observed discrete line distributions are also changing, as shown in Fig. 2(b). Herein, continuously tuning pressure can be achieved by the PZT-driven DAC device from 0.88 to 2.07 GPa for the first step (corresponding to PZT voltage 0–200 V). Then the DAC device was warmed up to the room temperature, and a new initial pressure value was exerted. After that, the DAC was cooled down to 20 K again and the next round of low-temperature pressure tuning and measurements starts, with a corresponding pressure range of 2.92–4.21 GPa. Figure 2(b) clearly demonstrates that with increasing pressure, 2D exciton and localized L exciton peak energies show blueshifts, as indicated by the dashed lines for eye guidelines,

*xmdou04@semi.ac.cn
†bqsun@semi.ac.cn

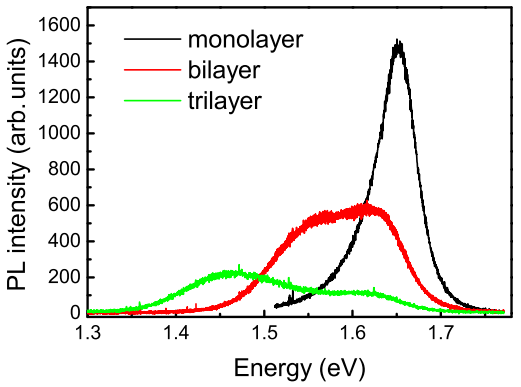

FIG. 1. PL spectra of monolayer, bilayer, and trilayer WSe_2 measured at room temperature.

and corresponding peak intensities gradually decrease. They become invisible at a pressure of approximately 1.62 GPa and many discrete lines emerge with further increasing pressure. It is noticed that the discrete lines distribute within the energy region of the broad L band (1.6–1.7 eV) or at the lower energy side ($h\nu$ below 1.6 eV). The diminished or suppressed 2D exciton and L exciton emissions imply that the pressure-induced defect states tend to trap more excitons and give rise to the discrete emission lines or an ensemble of discrete emission lines, as shown in Fig. 2 and also in Fig. 3(a). It is noticeable that, as indicated in Fig. 2, the discrete lines or broad envelope band composed of discrete lines show a redshift under pressures.

According to the peak energy position relative to the L excitons, these discrete emission lines can be divided into two groups, i.e., peak energies below and above 1.6 eV. One group

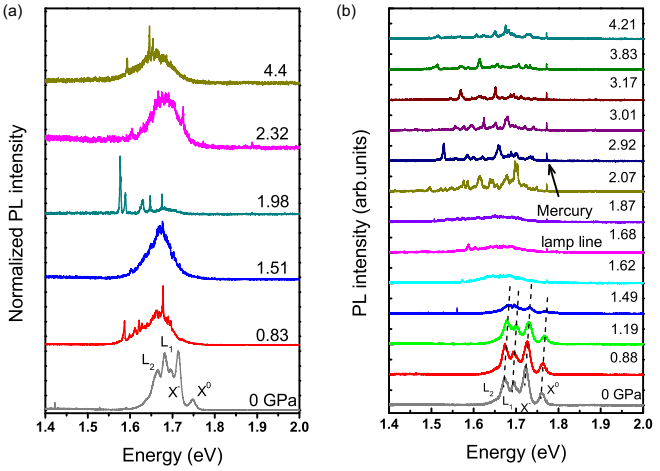

FIG. 2. (a) Normalized PL spectra measured at the pressures of 0, 0.83, 1.51, 1.98, 2.32, and 4.4 GPa, respectively, with an excitation power of 20 μW. A typical PL spectrum at zero pressure is 2D exciton X^0, 2D charged exciton X^- emissions, and localized excitonic L_1 and L_2 emissions. (b) PL spectra under pressures for the sample 2 at an excitation power of 45 μW, showing blueshifting of X^0, X^-, L_1, and L_2 peak energies as well as an emergence of the discrete lines. The black dashed lines are eye guidelines for the pressure response of X^0, X^-, L_1, and L_2 exciton peak energies, respectively.

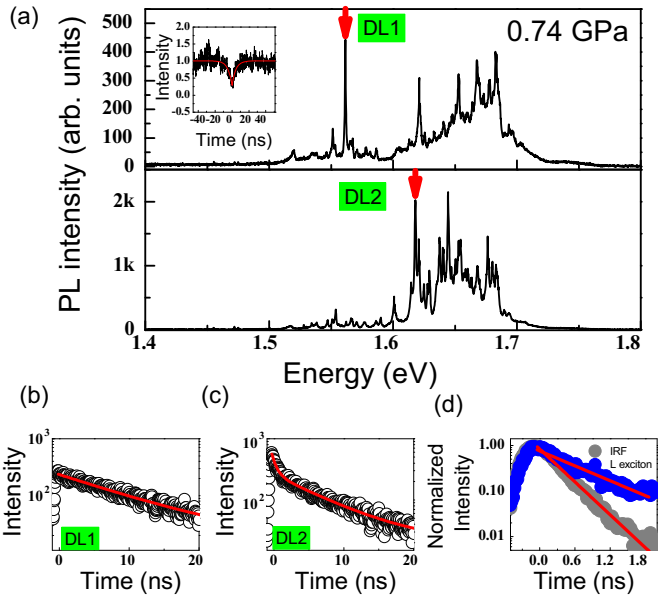

FIG. 3. (a) PL spectra of discrete line emissions at a pressure of 0.74 GPa, corresponding to two different laser excitation spots on the flake. DL1 and DL2 were used for time-resolved PL measurements. Inset: The measured $g^2(\tau)$ of DL1 and DL2, corresponding to $g^2(0)$ of 0.29 ± 0.02 and 0.28 ± 0.07, respectively. (b), (c) TR-PL spectra expressed in logarithmic coordinates, were measured by time-correlated single photon counting for discrete lines DL1 and DL2, respectively. (d) Time-resolved PL spectra at zero pressure for L_2 exciton emission (blue circles). The gray circles correspond to the IRF.

of peaks is located below 1.6 eV, which is lower than the L broadband; another group of discrete line peaks are above 1.6 eV, i.e., their energies are nearly overlapped with the L broadband seen at low pressure, as represented by DL1 and DL2 marked in Fig. 3(a) (sample 3), respectively. The single photon emission characteristic of both lines is confirmed by using second-order correlation function $g^{(2)}(\tau)$, as depicted in the insets of Fig. 3(a). In addition, the time-resolved PL measurement is applied to characterize the dynamic behavior of individual spectral lines. Figures 3(b) and 3(c) show the exciton decay curves of DL1 and DL2, respectively. It clearly exhibits that DL1 has a single exponential decay with a lifetime of 10.3 ± 0.5 ns. However, there are two decay times for the DL2, corresponding to the lifetimes of $\tau_1 = 0.62 \pm 0.03$ and $\tau_2 = 7.2 \pm 0.3$ ns, respectively. Here, an exciton decay time of a few nanoseconds of a discrete line is in agreement with the typical value for the quantum emitters in 2D materials [3,10]. Instead, the reported decay time of the broad L excitons is shorter, from 10 ps [16] to hundreds of picoseconds [17]. This means that the lifetime of discrete lines is about one or two orders longer than the lifetime of the broad L band emission. In fact, as shown in Fig. 3(d) the decay curve of L_2 emission is measured at zero pressure. A lifetime of 0.57 ± 0.03 ns of the decay curve is obtained by deconvolution of the PL curve from the instrument response function (IRF). Therefore, the time decay of DL2 may be related to two different kinds of exciton decay processes even if their emission energy is nearly overlapped at low pressure. It is noted that the lifetime τ_1 of

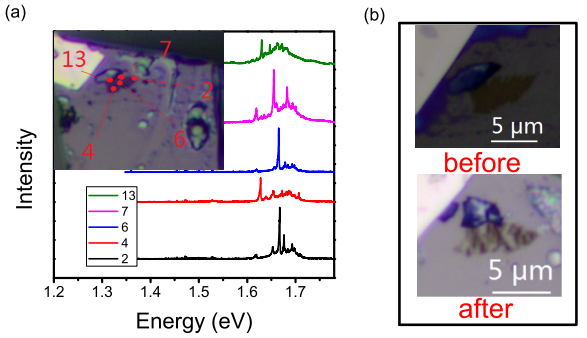

FIG. 4. (a) PL spectra and corresponding laser excitation spots on the monolayer flake at 1.1 GPa and 20 K through 50× objective. (b) Optical microscope images obtained before applying pressure and after releasing pressure at room temperature through 100× objective.

DL2 has the same order as the L_2 exciton. Thus, the detected signal of DL2 may be partly mixed with some contribution of "residual" L band emission; the fast decay process of DL2 can be attributed to the radiative recombination of L excitons instead of a quantum emitter.

To obtain spatial distributions of the discrete lines, PL mapping spectra are obtained at a pressure of 1.1 GPa, as shown in Fig. 4(a) (sample 4), together with an optical images obtained by 50× objective at 20 K. Here, it clearly exhibits that discrete lines emerge and have different distributions corresponding to the different spatial spots of the laser focus. This means that the discrete lines can be observed at the edges (marked by numbers of 2, 4, and 7) or central positions (marked by numbers of 6 and 13) of the flake. Furthermore, by carefully checking the microscope images of the monolayer flake by 100× objective at room temperature before and after applied pressures, it is found that cracks and wrinkles occur on the monolayer flake after releasing pressure, as shown in Fig. 4(b). Cracks appearing on the monolayer WSe_2 can result in dangling bonds or even reconstruction of the flake edges which are considered to form the deep levels below the band edge [18].

To inspect the pressure-induced shifts of emission peaks 2D-X^0, 2D-X^-, and L excitons, as well as of the discrete lines in detail, an *in situ* tunable pressure on the 2D flake has been exerted by using a PZT actuator-driven DAC device. The measured PL peak energies under high pressure show a blueshift for the 2D-X^0, 2D-X^-, and L excitons, and the corresponding PL intensity decreases gradually with increasing pressure, as shown in Fig. 5(a) (sample 2). The detailed experimental data of the PL peak energies as a function of pressure are plotted in Fig. 5(b), together with the data at zero pressure. All of these exciton peaks show blueshift with increasing pressure. The linear functions are employed to fit the data and the obtained the PCs are $14.7 \pm 0.2, 13.0 \pm 0.6, 14.4 \pm 0.8$, and 13.3 ± 0.5 meV/GPa for X^0, X^-, L_1, and L_2 excitons, respectively. The PC of the X^0 peak reflects a blueshift rate of band edge of the direct K-K interband transition in the Brillouin zone [19–22]. Here, the PC of X^0 of monolayer WSe_2 at low temperature is nearly a half of the value for 2D-X^0 at room temperature reported elsewhere [23]. The discrepancy in the PC values obtained at different temperatures is not understood at the

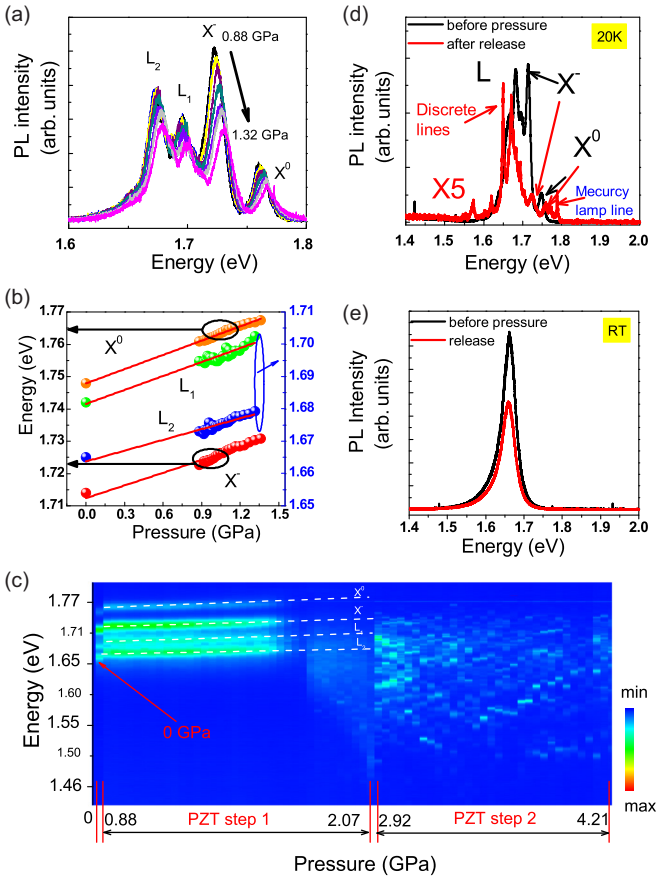

FIG. 5. (a) PL spectra response to the pressure ranging from 0.88 to 1.32 GPa for X^0, X^-, L_1, and L_2 exciton emission energies. (b) PL peak energies of X^0, X^-, L_1 and L_2 excitons as a function of pressure. The obtained pressure coefficients are $14.7 \pm 0.2, 13.0 \pm 0.6, 14.4 \pm 0.8$, and 13.3 ± 0.5 meV/GPa for X^0, X^-, L_1, and L_2 excitons, respectively. (c) Color-coded PL intensity and peak energy shift as a function of pressure. The white dashed lines are eye guidelines for the pressure response of X^0, X^-, L_1, and L_2 exciton peak energies, respectively. (d) PL spectra measured before applied pressure and after releasing the pressure at 20 K. (e) PL spectra measured before applied pressure and after releasing the pressure at room temperature.

moment. By comparing the PC of L_1 and L_2 excitons with that of X^0, it is found that defect-level-bound L_1 and L_2 excitons have nearly the same blueshift rate as X^0, suggesting that the related defect levels should correspond to the hydrogenlike shallow impurities. Figure 5(c) shows the color-coded PL intensities and peak energy shifts as a function of pressure. It is noticeable that 2D exciton and L exciton peak energies show nearly the same blueshift rate. With the suppression of 2D exciton and L exciton emissions, an ensemble of discrete lines or discrete lines emerge at the lower energy side for the PZT tuning step 1 (0.88–2.07 GPa). Much more clearly, individual lines can be observed at the second PZT tuning step (2.92–4.21 GPa). The spectral range of the discrete lines has a broader energy distribution. Specifically, it extends to the lower energy side at higher pressure. This kind of pressure-induced behavior is contrary to the way of response for direct band excitons (X^0 and X^-) and shallow-donor-bound L excitons under pressure (see the white dashed lines for eye guidelines). It is known

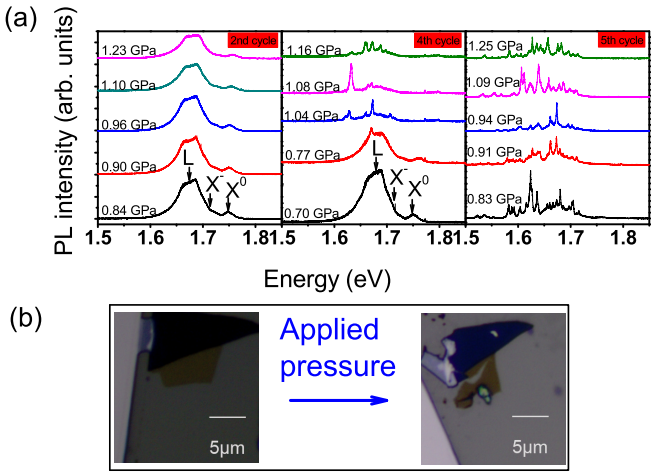

FIG. 6. (a) PL spectral evolution as a response to the pressure for the second, fourth, and fifth periods of pressure-tuning cycles obtained by *in situ* tuning the pressure through a piezoelectric actuator. (b) Optical microscope images obtained before applying pressure (left) and after releasing the pressure (right).

that the shift of shallow levels follows the conduction band edge under pressure, while the deep levels have a much less pressure-induced shift and normally show a strongly sublinear change with pressure [24,25]. Thus, based on the observed weak pressure response or redshift of the discrete lines, together with a longer decay time, showing a characteristic of stronger bounding from the defect state, the discrete line emissions are attributed to the exciton emissions bound to the deep-level defects which have a larger degree of atomiclike character and a stronger localization effect on excitons.

Accompanied with the appearance of discrete emitters, it is noted that the 2D excitons are simultaneously weakened or even disappear, as shown in Figs. 5(c) and 6(a) (sample 5). It is very similar to what was reported for the quantum emitters observed at the edge of etched holes, at the wrinkle on the flakes, or at the edge of flakes [1,10]. It can be assumed to be a result of the competition between different kinds of radiative recombination. The 2D excitons and weakly bounded L excitons are more easily trapped by strong localization centers newly created by hydrostatic pressure. Spatially, it is known that the discrete lines occur often at the edges of flakes and the regions of high strain gradient [2,9–11]. We find that for most studied samples 2D exciton peaks disappear at a pressure of ~0.6–1.5 GPa at the first cycle of the *in situ* pressure-changing process. This characteristic is relevant of pressure-induced cracks on the samples which may be a random process, directly resulting in a decrease and quenching of 2D exciton emissions corresponding to different pressures. After releasing the pressure to zero, PL is checked again at 20 K, showing an obvious change, as indicated by the red line in Fig. 5(d). Here, peaks of 2D X^0 and X^- are still visible and show a blueshift corresponding to the peaks before applied pressure. Peak blueshift of zero pressure PL spectra implies an existence of the residual strains on the sample. A similar strain-induced shifting of 2D excitons was found in Refs. [9,10]. However, at room temperature, the measured PL spectrum after releasing the pressure to zero, as shown in Fig. 5(e), exhibits a typical PL characteristic of monolayer WSe_2. We find, actually, that for all studied samples, after releasing the pressure to zero, the sample PL spectra show similar characteristics observed at low [see Fig. 5(d)] or room temperature [see Fig. 5(e)]; even the samples have been cracked seriously.

To further inspect the change in 2D and L exciton emissions, as well as the emergence of discrete emitters under pressure, several runs of pressure-tuning cycles are applied successively. The PL measurements after the second, fourth, and fifth periods of pressure-tuning cycles have been completed on the same location of the sample with the *in situ* pressure-tuning method, as indicated in Fig. 6(a). It is demonstrated that with increasing pressure-tuning cycles the 2D-X^0, 2D-X^-, and L exciton emissions become weaker and then even disappear. Then discrete emission lines appear and can be well recognized. It can be seen from the fourth and fifth applied pressure cycles that with increasing pressure, old emission lines die off quickly and some new ones emerge. This is assumed to directly result in an obvious difference between comblike emission spectra at different pressures. Comparing the optical microimages shown in Fig. 6(b) taken before and after pressure, residual strains or cracks have been found. A similar effect was reported to occur after a high-temperature annealing treatment of samples [26]. The pressure-induced change of the samples is the emerging of cracks, which results in much more edge states responsible for the discrete line emissions. The appearance of more defect states below the band edge will trap the occupied 2D and L excitons, i.e., suppression of 2D and L exciton emissions observed. This is a physical process due to the fact that at room temperature the sample PL spectrum recovers its typical PL characteristic and even at low temperature, the corresponding 2D excitons can still be observed. In addition, it is not a phase transition process owing to its transition pressure of ~38 GPa [27,28].

Summarizing the previous discussions, we can illustrate the optical transitions of X^0, X^-, and L excitons as well as deep-level defects by a simple schematic diagram in Figs. 7 (a) and 7(b), respectively. Figure 7(a) shows typical PL emissions of X^0, X^-, and L excitons observed at low temperature and normal pressure; whereas, the discrete lines from deep levels proved to be difficult to observe in the exfoliated monolayer

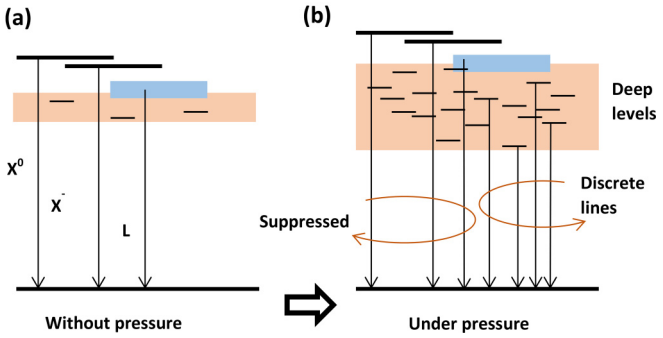

FIG. 7. (a) Schematic diagram of the optical transitions of X^0, X^-, and L excitons at low temperature and normal pressure. (b) Emissions of the X^0, X^-, and L excitons are suppressed under pressure, and new discrete lines emerge related to the optical transitions of deep levels.

WSe_2, although a few groups were reported on the discrete emission lines at the edges of the flakes [1–9]. However, it is easier to observe the discrete lines as the pressure is applied. The applied pressure, on the one hand, leads to the blueshifts of the PL peak energies of the band excitons (X^0 and X^-) and shallow-donor-bound L excitons, along with the decrease of the PL intensities and suppression of the exciton emissions. On the other hand, the pressure can cause the monolayer sample to crack, in which many new defect states (deep levels) emerge at the edges of the cracked sample, as shown in Fig. 7(b). The pressure behaviors of the ensembles of the defect states seem to be less sensitive or redshift.

In summary, we report an effective method to give rise to single photon emission lines in 2D WSe_2 material by applying hydrostatic pressure. We find that the 2D-X^0 and 2D-X^- exciton emissions are quenched at high pressure. The pressure-induced residual strains or cracks on the sample can be responsible for the emergence of single photon emissions and the quenching of 2D exciton emissions. Based on nearly the same pressure-induced blueshift rate for both 2D excitons and L excitons, the defect states which bound L excitons are attributed to shallow impurity levels; whereas, the emergent discrete line emissions are demonstrated to be less pressure sensitive. In addition, the exciton decay times of these lines are longer, to be approximately 10 ns. These characteristics reveal that excitons of discrete line emissions should be bound to the deep-level defects. The report here should be significant for searching single photon emission based on defect engineering in 2D materials. The exceptionally large exciton g factor of discrete lines reported in monolayer WSe_2 may be also related to the atomiclike character of the deep-level defects [1–3].

This work was supported by the National Key Basic Research Program of China (Grant No. 2013CB922304), the National Key Research and Development Program of China (Grant No. 2016YFA0301202), and the National Natural Science Foundation of China (Grants No. 11474275 and No. 11574301).

[1] A. Srivastava, M. Sidler, A. V. Allain, D. S. Lembke, A. Kis, and A. Imamoglu, Nat. Nanotechnol. **6**, 491 (2015).
[2] M. Koperski, K. Nogajewski, A. Arora, V. Cherkez, P. Mallet, J. Y. Veuillen, J. Marcus, P. Kossacki, and M. Potemski, Nat. Nanotechnol. **6**, 503 (2015).
[3] Y. M. He, G. Clark, J. R. Schaibley, Y. He, M. C. Chen, Y. J. Wei, X. Ding, Q. Zhang, W. Yao, X. Xu, C. Y. Lu, and J. W. Pan, Nat. Nanotechnol. **6**, 497 (2015).
[4] S. Kumar, M. Brotóns-Gisbert, R. Al-Khuzheyri, A. Branny, G. Ballesteros-Garcia, J. F. Sánchez-Royo, and B. D. Gerardot, Optica **8**, 882 (2016).
[5] P. Tonndorf, R. Schmidt, R. Schneider, J. Kern, M. Buscema, G. A. Steele, A. Castellanos-Gomez, H. S. J. van der Zant, S. Michaelis de Vasconcellos, and R. Bratschitsch, Optica **4**, 347 (2015).
[6] C. Chakraborty, L. Kinnischtzke, K. M. Goodfellow, R. Beams, and A. N. Vamivakas, Nat. Nanotechnol. **6**, 507 (2015).
[7] K. F. Mak, and J. Shan, Nat. Photonics **4**, 216 (2016).
[8] T. T. Tran, K. Bray, M. J. Ford, M. Toth, and I. Aharonovich, Nat. Nanotechnol. **1**, 37 (2016).
[9] A. Branny, G. Wang, S. Kumar, C. Robert, B. Lassagne, X. Marie, B. D. Gerardot, and B. Urbaszek, Appl. Phys. Lett. **108**, 142101 (2016).
[10] S. Kumar, A. Kaczmarczyk, and B. D. Gerardot, Nano Lett. **11**, 7567 (2015).
[11] J. Kern, I. Niehues, P. Tonndorf, R. Schmidt, D. Wigger, R. Schneider, T. Stiehm, S. Michaelis de Vasconcellos, D. E. Reiter, T. Kuhn, and R. Bratschitsch, Adv. Mater. **33**, 7101 (2016).
[12] X. F. Wu, X. M. Dou, K. Ding, P. Y. Zhou, H. Q. Ni, Z. C. Niu, D. S. Jiang, and B. Q. Sun, Appl. Phys. Lett. **103**, 252108 (2013).
[13] A. M. Jones, H. Yu, N. J. Ghimire, S. Wu, G. Aivazian, J. S. Ross, B. Zhao, J. Yan, D. G. Mandrus, D. Xiao, W. Yao, and X. Xu, Nat. Nanotechnol. **9**, 634 (2013).
[14] C. R. Zhu, K. Zhang, M. Glazov, B. Urbaszek, T. Amand, Z. W. Ji, B. L. Liu, and X. Marie, Phys. Rev. B **90**, 161302(R) (2014).
[15] A. Srivastava, M. Sidler, A. V. Allain, D. S. Lembke, A. Kis, and A. Imamoğlu, Nat. Phys. **2**, 141 (2015).
[16] G. Wang, L. Bouet, D. Lagarde, M. Vidal, A. Balocchi, T. Amand, X. Marie, and B. Urbaszek, Phys. Rev. B **90**, 075413 (2014).
[17] Y. You, X.-X. Zhang, T. C. Berkelbach, M. S. Hybertsen, D. R. Reichman, and T. F. Heinz, Nat. Phys. **6**, 477 (2015).
[18] J. Kunstmann, T. B. Wendumu, and G. Seifert, Phys. Status Solidi B **254**, 1600645 (2016).
[19] C.-H. Chang, X. Fan, S.-H. Lin, and J.-L. Kuo, Phys. Rev. B **88**, 195420 (2013).
[20] M. Pena-Alvarez, E. del Corro, A. Morales-Garcia, L. Kavan, M. Kalbac, and O. Frank, Nano Lett. **5**, 3139 (2015).
[21] S. B. Desai, G. Seol, J. S. Kang, H. Fang, C. Battaglia, R. Kapadia, J. W. Ager, J. Guo, and A. Javey, Nano Lett. **8**, 4592 (2014).
[22] C. R. Zhu, G. Wang, B. L. Liu, X. Marie, X. F. Qiao, X. Zhang, X. X. Wu, H. Fan, P. H. Tan, T. Amand, and B. Urbaszek, Phys. Rev. B **88**, 121301(R) (2013).
[23] Y. Ye, X. Dou, K. Ding, D. Jiang, F. Yang, and B. Sun, Nanoscale **20**, 10843 (2016).
[24] B. H. Cheong and K. J. Chang, Phys. Rev. Lett. **71**, 4354 (1993).
[25] W. P. Roach, M. Chandrasekhar, H. R. Chandrasekhar, F. A. Chambers, and J. M. Meese, Semicond. Sci. Technol. **4**, 290 (1989).
[26] H. Y. Nan, Z. L. Wang, W. H. Wang, Z. Liang, Y. Lu, Q. Chen, D. W. He, P. H. Tan, F. Miao, X. R. Wang, J. L. Wang, and Z. H. Ni, ACS Nano **6**, 5738 (2014).
[27] B. Liu, Y. H. Han, C. X. Gao, Y. Z. Ma, G. Peng, B. J. Wu, C. L. Liu, Y. Wang, T. J. Hu, X. Y. Cui, W. B. Ren, Y. Li, N. N. Su, H. W. Liu, and G. T. Zou, J. Phys. Chem. C **33**, 14251 (2010).
[28] E. Selvi, R. Aksoy, R. Knudson, and Y. Ma, J. Phys. Chem. Solids **9**, 2311 (2008).